

## ARTICLE

# Preclinical Investigation of the Novel Histone Deacetylase Inhibitor AR-42 in the Treatment of Cancer-Induced Cachexia

Yu-Chou Tseng\*, Samuel K. Kulp\*, I-Lu Lai, En-Chi Hsu, Wei A. He, David E. Frankhouser, Pearly S. Yan, Xiaokui Mo, Mark Bloomston, Gregory B. Lesinski, Guido Marcucci, Denis C. Guttridge, Tanios Bekaii-Saab, Ching-Shih Chen

**Affiliations of authors:** Division of Medicinal Chemistry and Pharmacognosy, College of Pharmacy (YCT, SKK, ILL, ECH, CSC), Department of Molecular Virology, Immunology, and Medical Genetics (WAH, DCG), Department of Surgery (MB), Department of Internal Medicine (GBL, GM, TBS), and Center for Biostatistics (XM), College of Medicine, and Genomics Shared Resource (DEF, PSY), The Comprehensive Cancer Center, The Ohio State University, Columbus, OH; Institute of Basic Medical Sciences, National Cheng-Kung University, Tainan, Taiwan (CSC); Institute of Biological Chemistry, Academia Sinica, Taipei, Taiwan (CSC).

\*Authors contributed equally to this work.

**Correspondence to:** Tanios Bekaii-Saab, MD, FACP, The Ohio State University - James Cancer Hospital, A454 Starling-Loving Hall, 320 West 10th Avenue, Columbus, OH 43210 (e-mail: [Tanios.Saab@osumc.edu](mailto:Tanios.Saab@osumc.edu)) and Ching-Shih Chen, PhD, The Ohio State University College of Pharmacy, 336 Parks Hall, 500 W. 12th Avenue, Columbus, OH 43210 (e-mail: [chen.844@osu.edu](mailto:chen.844@osu.edu)).

## Abstract

**Background:** Cancer cachexia is a debilitating condition that impacts patient morbidity, mortality, and quality of life and for which effective therapies are lacking. The anticachectic activity of the novel HDAC inhibitor AR-42 was investigated in murine models of cancer cachexia.

**Methods:** The effects of AR-42 on classic features of cachexia were evaluated in the C-26 colon adenocarcinoma and Lewis lung carcinoma (LLC) models. Effects on survival in comparison with approved HDAC inhibitors (vorinostat, romidepsin) were determined. The muscle metabolome and transcriptome (by RNA-seq), as well as serum cytokine profile, were evaluated. Data were analyzed using mixed effects models, analysis of variance, or log-rank tests. All statistical tests were two-sided.

**Results:** In the C-26 model, orally administered AR-42 preserved body weight ( $23.9 \pm 2.6$  grams, AR-42-treated;  $20.8 \pm 1.3$  grams, vehicle-treated;  $P = .005$ ), prolonged survival ( $P < .001$ ), prevented reductions in muscle and adipose tissue mass, muscle fiber size, and muscle strength and restored intramuscular mRNA expression of the E3 ligases MuRF1 and Atrogin-1 to basal levels ( $n = 8$ ). This anticachectic effect, confirmed in the LLC model, was not observed after treatment with vorinostat and romidepsin. AR-42 suppressed tumor-induced changes in inflammatory cytokine production and multiple procachexia drivers (IL-6, IL-6R $\alpha$ , leukemia inhibitory factor, Foxo1, Atrogin-1, MuRF1, adipose triglyceride lipase, uncoupling protein 3, and myocyte enhancer factor 2c). Metabolomic analysis revealed cachexia-associated changes in glycolysis, glycogen synthesis, and protein degradation in muscle, which were restored by AR-42 to a state characteristic of tumor-free mice.

**Conclusions:** These findings support further investigation of AR-42 as part of a comprehensive therapeutic strategy for cancer cachexia.

Received: September 17, 2014; Revised: March 9, 2015; Accepted: August 31, 2015

© The Author 2015. Published by Oxford University Press. All rights reserved. For Permissions, please e-mail: [journals.permissions@oup.com](mailto:journals.permissions@oup.com).

Cachexia is characterized by loss of skeletal muscle mass that is not reversed by nutritional support, leading to pronounced weight loss that severely impacts patient morbidity and mortality (1,2). Cachexia occurs in 70% of advanced cancer patients and is prevalent in pancreas and gastro-esophageal cancers (3). Thus, the development of effective therapies for cancer cachexia is clearly warranted. With the advent of new tools to identify pro-cachectic factors and their effects on skeletal muscle, important advances in understanding the underlying mechanisms that regulate muscle atrophy in cancer have been made (4). As a result, signaling mechanisms by which cytokines and systemic inflammation regulate muscle wasting have been identified (1). Translating these findings into effective therapies proves challenging (5), and they are still lacking (5,6).

Recently, histone deacetylase (HDAC)1, a class I HDAC, was identified as an important mediator of skeletal muscle atrophy associated with disuse and nutrient deprivation (7). This finding suggests the use of class I HDAC inhibitors as a viable pharmacologic approach for the treatment of muscle atrophy. Here, we report the comprehensive evaluation of the anticachectic activity of AR-42 (formerly, OSU-HDAC42 [8–11]), a novel class I/II HDAC inhibitor currently in clinical trials, in two murine models of cancer cachexia, the colon-26 (C-26) adenocarcinoma and Lewis lung carcinoma (LLC) models.

## Methods

Information on cell culture, animals, HDAC inhibitors, antibodies, and methods for grip strength measurement, immunoblotting, quantitative real-time polymerase chain reaction (qRT-PCR), and RNA-seq library generation and data analysis are included in the [Supplementary Methods](#) (available online).

## Cancer Cachexia Models

All animal studies were conducted according to protocols approved by The Ohio State University Institutional Animal Care and Use Committee. For the C-26 model, tumors were established by subcutaneous injection of C-26 cells ( $0.5 \times 10^6$  cells in 0.1 mL) into the right flank of male CD2F1 mice (approximately 6 weeks of age; Harlan Laboratories, Indianapolis, IN) (12). Tumor-bearing and tumor-free mice, the latter serving as noncachectic controls, were randomized into groups that received either AR-42 (50 mg/kg, p.o. by gavage, every other day) or vehicle (0.5% methylcellulose [w/v] and 0.1% Tween-80 [v/v] in sterile water) starting six days after cell injection. To investigate the effect of delayed treatment, treatments were started six, 10, and 12 days after cancer cell injection. To compare AR-42 with other HDAC inhibitors, additional groups of C-26 tumor-bearing mice were treated with vorinostat (50 mg/kg, p.o., once daily) and romidepsin (0.6 mg/kg; i.p., twice weekly). To investigate the effects of AR-42 on histone H3 acetylation in skeletal muscle and epididymal fat, tissues were harvested from C-26-tumor bearing mice six hours after drug treatment on Day 6, 10, and 12 after tumor cell injection. For the LLC model, subcutaneous tumors were established in male C57BL/6 mice (approximately 6 weeks of age; Harlan) by injection of  $0.5 \times 10^6$  LLC cells into the right flank. Treatment with AR-42 and vehicle was performed as for the C-26 model. In both models, body weights and food consumption were monitored daily and tumor size was measured no less than every two days. For all animal experiments, the study endpoint was 12, 15, or 17 days, except for the survival study, in which mice were killed when they reached criteria for removal as dictated by the animal use protocol. Mice were fasted for two

hours prior to death, at which time tissues were collected for analysis. Muscle samples were frozen in liquid nitrogen-chilled 2-methylbutane and then stored at  $-80^\circ\text{C}$  until analysis.

## Grip Strength Measurement

Forelimb grip strength was measured mice using a Digital Grip Strength Meter (Columbus Instruments, Columbus, OH). For each mouse, grip strength was defined as the average of five measurements.

## Morphometric Analysis of Muscle Fiber Size

Ten  $\mu\text{m}$  sections were cut from frozen skeletal muscle samples using a cryostat (Leica Microsystems, Buffalo Grove, IL) and then stained with hematoxylin and eosin. Images were captured using an Olympus BX51 microscope (Olympus America, Inc., Waltham, MA), and muscle fiber cross-sectional areas were determined using Olympus CellSens 1.11 software. Measurements were obtained from five different sections of muscle from each of five mice from each group.

## Metabolomic and Cytokine Profiling

Gastrocnemius muscles and sera were collected at Day 17 post-cell injection from each treatment group ( $n = 8/\text{group}$ ). Muscle was submitted to Metabolon, Inc. (Durham, NC) for metabolomic analysis of 270 metabolic intermediates via proprietary mass spectrometry platforms. Serum was submitted to Eve Technologies (Calgary, Alberta, Canada) for analysis of 32 cytokines using a mouse cytokine array (32-plex panel).

## Statistical Analysis

Analysis was conducted by using SAS 9.3 software (SAS, Inc; Cary, NC). All variables included in the statistical analyses were continuous, and all tests performed were two-sided. For the experiments with repeated measures, data were analyzed by mixed effect models, accounting for the association of the same measure at different time points from the same subject. These models included treatment and days of the treatment as fixed factors, and the intercept of an individual subject was considered as a random effect (13). For experiments involving independent groups with just one measure for each mouse, data were analyzed by analysis of variance (ANOVA). For the time-to-event experiment, the differences in survival functions were compared by log-rank tests. Multiplicities were adjusted by Holm's method to control the overall family-wise error rate at 0.05 (14). The differentially expressed genes identified by RNA-seq data were analyzed by using Ingenuity Pathway Analysis (IPA) software (Ingenuity Systems, Redwood City, CA). Only genes with greater than four-fold change and *P* values of less than .05 were selected for pathway analysis.

## Results

### Effects of AR-42 on Cancer Cachexia in the C-26 Colon Adenocarcinoma Model

Starting six days after injection of C-26 cells, when palpable tumors had formed, mice were treated with AR-42 (50 mg/kg) or vehicle every other day. As expected, body weights in the vehicle-treated group decreased sharply starting at Day 12, while

AR-42-treated mice maintained weight at levels comparable with that of tumor-free controls (mean ± SD [grams], Day 14: control, 25.3±1.1; vehicle, 23.4±1.4; AR-42, 25.9±2.6; *P* = .045, vehicle vs AR-42; Day 15: vehicle, 22.1±1.3; AR-42, 25.0±2.6; *P* = .003) (Figure 1A, left). By day 15, the magnitude of the weight

loss, after deducting tumor weights, reached greater than 20% for the vehicle-treated group, but only 6% for AR-42-treated mice (mean ± SD [grams], vehicle, 20.8±1.3; AR-42, 23.9±2.6; *P* = .005) (Figure 1A, center). This effect could not be attributed to decreased tumor burden (Figure 1A, right) or to increased

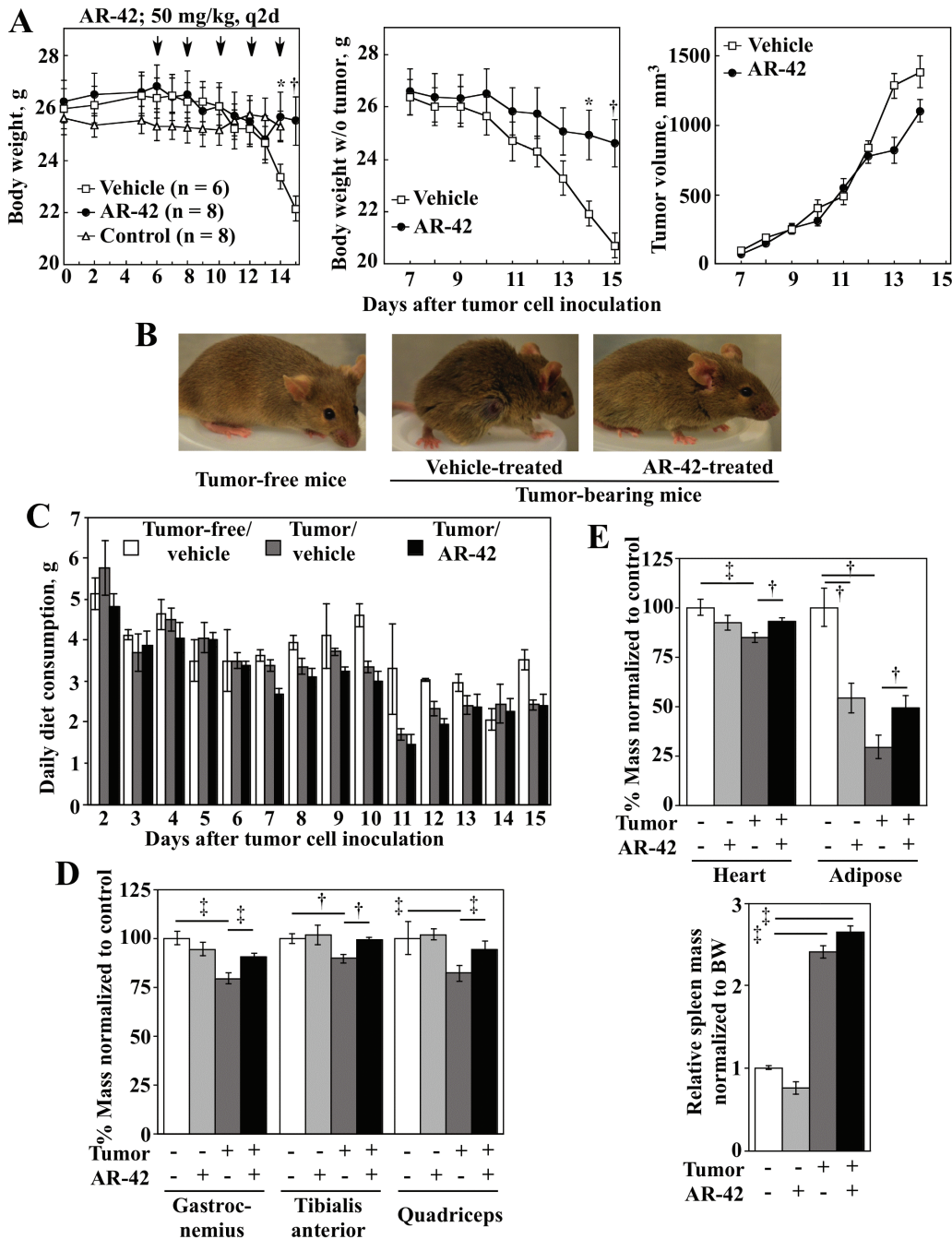


**Figure 1.** Effects of AR-42 on cancer cachexia-associated losses of body weight and skeletal muscle mass in C-26 tumor-bearing mice. **A**) Changes in total weight (left, tumor included) and body weight (center, tumor excluded) during the 15-day study in vehicle-treated tumor-free mice (Control) vs tumor-bearing mice treated with vehicle (Vehicle) or oral AR-42 at 50mg/kg every other day (AR-42). Arrows indicate the times of AR-42 treatment. Right, lack of suppressive effect of AR-42 on tumor growth in C-26 tumor-bearing mice. Data are presented as means ± SD and were analyzed with mixed effects model incorporating repeated measures for each subject with treatment and days as fixed factors. \**P* < .05; †*P* < .01 (AR-42 vs Vehicle). **B**) Photographs of representative mice from each group at the study endpoint depicting the therapeutic effect of AR-42 on cancer cachexia in tumor-bearing mice, as manifested by normal posture, smooth haircoat, and better body condition, despite large tumor burdens. **C**) Average daily diet consumption among the three treatment groups in the course of study. Data are presented as means ± SD (*n* = 8). **D and E**) Effects of AR-42 on the weights of **(D)** hindlimb muscles, including gastrocnemius, tibialis anterior, and quadriceps, and **(E)** the heart, adipose tissue and spleen in tumor-free and tumor-bearing mice compared with those of vehicle-treated tumor-bearing and tumor-free mice. Data are presented as means ± SD (*n* = 8; †*P* < .01; ‡*P* < .001; analysis of variance). All statistical tests were two-sided.

food intake (Figure 1C), as AR-42 did not affect these parameters relative to the vehicle-treated group. The AR-42-treated mice, despite large tumor burdens, were alert, responsive, active, and lacked the hunched posture and rough haircoat observed in vehicle-treated counterparts (Figure 1B).

Indicative of cachexia, the weights of gastrocnemius, tibialis anterior, and quadriceps muscles from vehicle-treated tumor-bearing (tumor-bearing/vehicle) mice were reduced to (mean  $\pm$  SD)  $79.4 \pm 7.0$  ( $P < .001$ ),  $89.5 \pm 10.1$  ( $P = .004$ ), and  $81.9 \pm 4.8\%$  ( $P < .001$ ), respectively, of those from tumor-free control mice. In contrast, muscle weights in AR-42-treated tumor-bearing (tumor-bearing/AR-42) mice were preserved (mean  $\pm$  SD;  $90.4 \pm 5.1$ ,  $99.2 \pm 8.8$ , and  $94.2 \pm 8.0\%$ , respectively, of the tumor-free controls) (Figure 1D). Thus, AR-42 protected skeletal muscle against cancer-associated wasting in this model.

This protective effect extended to cardiac and adipose tissue weights, which were also reduced in tumor-bearing/vehicle mice (mean  $\pm$  SD,  $85.9 \pm 5.5$ ,  $P < .001$ , and  $29.3 \pm 6.0\%$ ,  $P < .001$ , of tumor-free control, respectively). AR-42 treatment diminished these losses (mean  $\pm$  SD,  $90.6 \pm 5.3\%$ , and  $47.7 \pm 13.5\%$  of tumor-free control;  $P = .006$  and  $.009$ , respectively, vs tumor-bearing/vehicle) (Figure 1E, upper). Interestingly, AR-42 itself reduced adipose tissue mass in tumor-free mice (mean  $\pm$  SD,  $54.0 \pm 16.9\%$  of tumor-free control,  $P = .001$ ) yet restored adipose tissue in tumor-bearing mice to a level comparable with that of tumor-free/AR-42 mice, a dichotomous effect suggesting its ability to maintain lipid homeostasis.

Splenomegaly is a feature of the C-26 model that results from expansion of myeloid-derived suppressor cells and other immune cells in the spleen (12,15). Spleen weight increased by  $2.4 \pm 0.4$ -fold in tumor-bearing/vehicle mice (mean  $\pm$  SD,  $P < .001$ ), but was unaffected by AR-42 ( $2.6 \pm 0.6$ -fold increase, tumor-bearing/AR-42) (Figure 1E, lower), suggesting that AR-42 acted predominantly on the muscle and adipose tissue rather than through an immunologic mechanism. This premise was supported by the increased acetylation of histone H3 in skeletal muscle and adipose tissue collected from AR-42-treated mice (Figure 2A), which was observed following the first dose of the drug on Day 6 and was maintained by the continued oral administration in both tumor-bearing and tumor-free mice.

The protective effect of AR-42 against muscle wasting was evident in the abrogation of cachexia-induced reduction in skeletal muscle fiber size. Tumor-bearing/vehicle mice exhibited a 48.2% decrease relative to the tumor-free control in mean cross-sectional area of muscle fibers at Day 15 ( $1297.6 \pm 638.8$  vs  $2503.5 \pm 917.5 \mu\text{m}^2$ ), which was restored by AR-42 ( $2146.3 \pm 923.4 \mu\text{m}^2$ ). The prominent shift in fiber size distribution to smaller cross-sectional area in cachectic muscles was reversed by AR-42 (Figure 2B).

### Effects of AR-42 and Other HDAC Inhibitors on Survival of C-26 Tumor-Bearing Mice

AR-42 was evaluated against two other HDAC inhibitors, vorinostat (16) and romidepsin (17), for effects on survival rates in C-26 tumor-bearing mice. AR-42 protected these mice from tumor-associated wasting, with 100% cumulative survival at Day 21 when tumor volume reached the threshold for removal from the study, while vorinostat and romidepsin showed limited or no appreciable protective effects on body weight (Figure 2C). Moreover, tumor-bearing/AR-42 mice were alert, responsive, active, and appeared healthy at 21 days, in contrast to vehicle- (Day 15), romidepsin- (Day 16), and vorinostat-treated mice (Day 18) (Supplementary Figure 1, available online).

### Differential Effects on E3 Ligase Expression in Skeletal Muscle

As skeletal muscle mass is regulated by a balance between protein synthesis and degradation, the differential anticachectic effect of AR-42 vs vorinostat and romidepsin may reflect differences in their ability to regulate pathways governing protein turnover. Indeed, among the three HDAC inhibitors, only AR-42 could restore mRNA expression of Atrogin-1 and MuRF1, two E3 ligases involved in ubiquitin-mediated skeletal muscle protein degradation (18,19), to basal levels ( $P < .001$  vs tumor-bearing/vehicle). Although vorinostat and romidepsin also reduced Atrogin-1 and MuRF1 mRNA expression in cachectic muscles (Atrogin-1/MuRF1: vorinostat,  $P < .001$ ; romidepsin,  $P = .016/.006$ ), they did so to a lesser extent than AR-42 (Figure 2D).

### Effect of AR-42 on Cancer Cachexia in the LLC Model

To confirm that the anticachectic activity of AR-42 was not specific to the C-26 model, it was also evaluated in the LLC model. As shown in Supplementary Figure 2 (available online), AR-42 protected LLC tumor-bearing C57BL/6 mice from loss of mass in all three muscle types examined (all  $P$  values  $< .05$ ,  $n = 8$ ).

### Effect of AR-42 on Metabolic Integrity of Muscle in Tumor-Bearing Mice

With cachexia, skeletal muscles undergo complex metabolic changes in response to tumor/host-derived inflammatory and neuroendocrine stressors (1). To investigate the effect of AR-42 on cachexia-induced shifts in metabolic phenotype in skeletal muscle, metabolic profiling was performed on gastrocnemius muscles collected from vehicle- or AR-42-treated tumor-free and C-26 tumor-bearing mice ( $n = 8$ /group).

In cachectic muscles, glucose and key glycolytic intermediates were decreased (Figure 3A), as were short-chain malto-oligosaccharides and glucose 1-phosphate (Figure 3B), suggesting perturbed glycolysis and depletion of glycogen stores. Indicative of increased muscle protein breakdown, free amino acids were elevated, including branched-chain amino acids and metabolites, such as kynurenine, *N*-acetyl-aspartyl-glutamate, and  $\gamma$ -aminobutyrate, which function in neurotransmission, and 2-hydroxybutyrate and ophthalmate, which are biomarkers for insulin resistance (20) and oxidative stress (21), respectively. In contrast, alanine, which is released from muscles to support liver gluconeogenesis, was reduced (Figure 4).

AR-42 reversed these cachexia-associated changes in glucose and amino acid metabolism and protein degradation. AR-42 restored glucose and glycolytic intermediates to levels similar to or above baseline levels detected in tumor-free/vehicle mice and replenished the glycogen metabolic intermediates (Figure 3). Elevated glucose was shunted into sorbitol-fructose biosynthesis and pentose phosphate pathways, leading to increased production of sorbitol, fructose, and ribose. Finally, the catabolic muscle phenotype was reversed in AR-42-treated mice in which free amino acids and metabolites were reduced to levels characteristic of a noncachectic state (Figure 4).

### Effects of AR-42 on Cytokine Profile and Muscle Transcriptome in Tumor-Bearing Mice

To shed light onto AR-42's anticachectic mechanism, sera and gastrocnemius muscle from vehicle- or AR-42-treated tumor-free and C-26 tumor-bearing mice were used for cytokine profiling and whole transcriptome shotgun sequencing (RNA-seq), respectively.

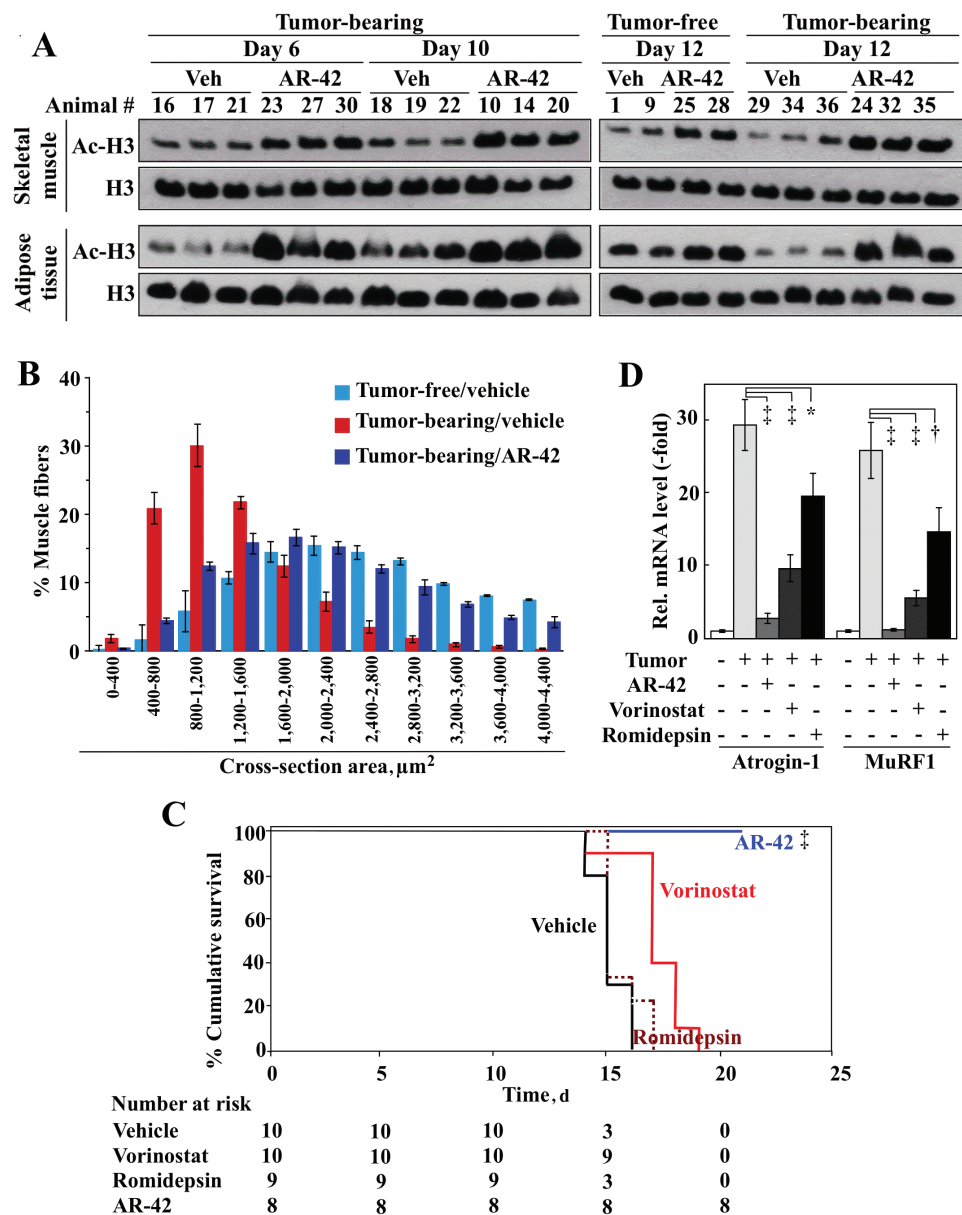


**Figure 2.** Effects of AR-42 on muscle fiber size and histone H3 acetylation status and survival relative to vorinostat and romidepsin in C-26 tumor-bearing mice. **A)** Western blot analysis of the effects of AR-42 on histone H3 acetylation in skeletal muscles and adipose tissues of C-26 tumor-bearing and/or tumor-free mice. Mice were treated orally with vehicle or AR-42 (50 mg/kg, p.o., every other day) as described in Figure 1A for up to 12 days post-tumor cell injection. Gastrocnemius muscles and epididymal adipose tissues were collected at six hours after treatment on Day 6, 10, and 12 post-tumor cell injection for evaluation of histone H3 acetylation. Tumor-free control mice were treated with vehicle or AR-42 in parallel for 12 days. The uncropped full images of these blots are shown in Supplementary Figure 4 (available online). **B)** The cross-sectional areas of muscle fibers in gastrocnemius muscles represented as a frequency histogram. Five sections from the gastrocnemius from each of five mice per treatment group were analyzed as described in the Methods section. Using multiple comparisons for the log-rank test, comparison between muscles from tumor-bearing/vehicle and tumor-bearing/AR-42 mice showed statistical significance ( $P < .001$ ). Data are presented as means  $\pm$  SD. **C)** Kaplan-Meier survival curves are shown for tumor-bearing mice treated with vehicle, vorinostat (50 mg/kg, p.o., daily), romidepsin (0.6 mg/kg, i.p., twice weekly), or AR-42 (50 mg/kg, p.o., every other day). Survival was defined as the time at which loss of body weight (tumor excluded) reached 20% of starting body weight, which served as a humane endpoint for removal from the study ( $\dagger P < .001$ , vehicle vs AR-42;  $n = 8$ ; log-rank test). **D)** Quantitative polymerase chain reaction analyses of the relative mRNA expression levels of Atrogin-1/MAFbx and MuRF1 in the skeletal muscles of vehicle-treated tumor-free mice ( $n = 6$ ) and tumor-bearing mice treated with AR-42 ( $n = 8$ ), vorinostat ( $n = 8$ ), or romidepsin ( $n = 5$ ) compared with that of vehicle-treated tumor-bearing mice ( $n = 8$ ) at 15 days after tumor cell injection. Data are presented as means  $\pm$  SD ( $*P < .05$ ;  $\dagger P < .01$ ;  $\ddagger P < .001$ ; analysis of variance). All statistical tests were two-sided.

### Cytokine Profiles

Of 32 cytokines examined (Supplementary Table 2, available online), IL-6 and leukemia inhibitory factor (LIF), two well-recognized cachexia drivers (22), were increased in the sera of tumor-bearing/vehicle mice ( $P < .001$  for both markers vs tumor-free/

vehicle mice) (Figure 5, Ai and ii), while no statistically significant differences were noted with other cytokines. AR-42 reduced IL-6 and LIF levels by 56 and 88%, respectively, in tumor-bearing mice (IL-6,  $P = .006$ ; LIF,  $P < .001$ ) compared with the vehicle-treated counterparts. Like serum IL-6, mRNA levels of IL-6 receptor alpha chain

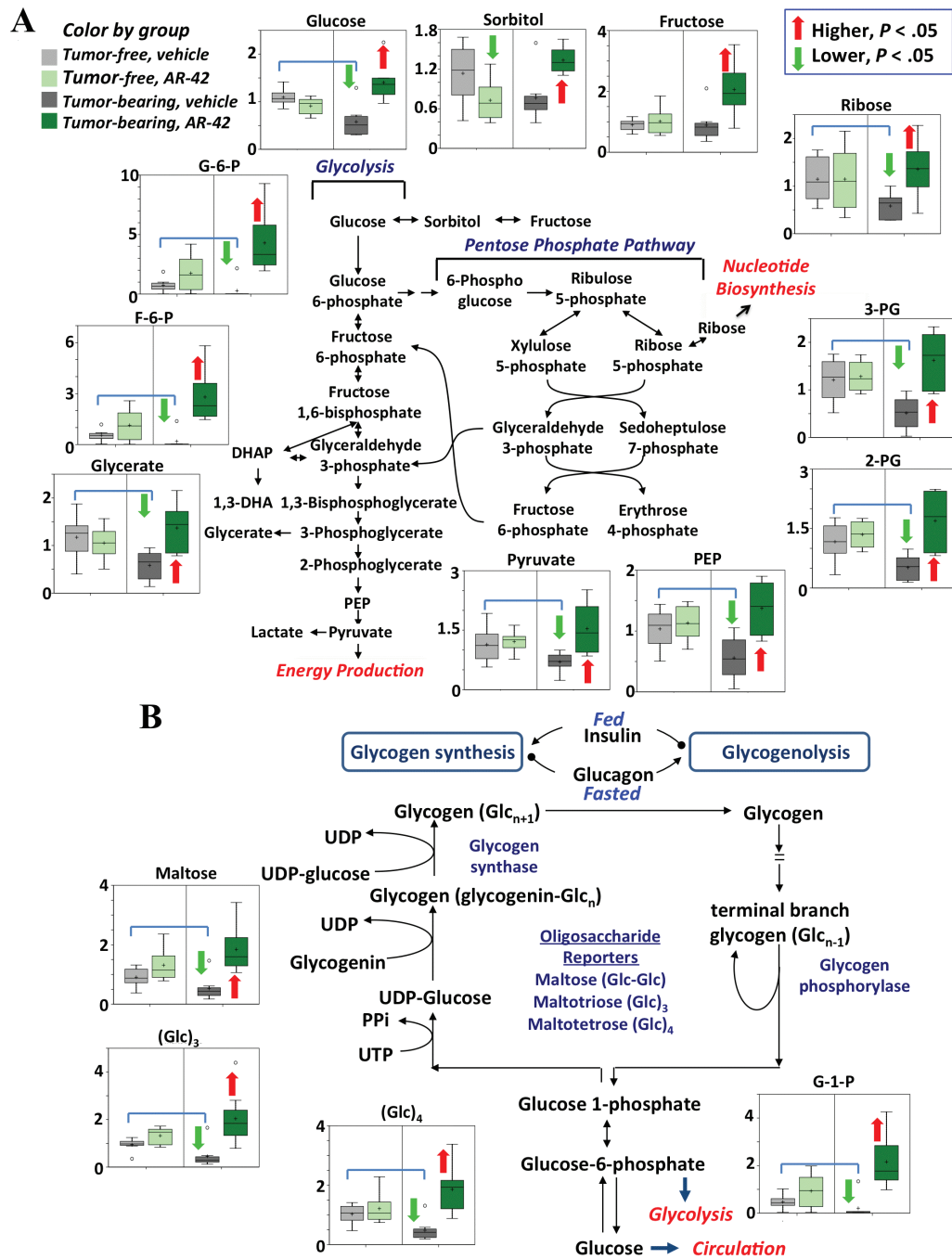


**Figure 3.** Effects of AR-42 on cachexia-associated glycolytic and glycogen metabolism signatures in skeletal muscle of C-26 tumor-bearing mice. Effects of AR-42 on the levels of intermediates associated with (A) glycolysis and alternative pathways of glucose metabolism and (B) glycogen metabolism in gastrocnemius muscles from tumor-free and tumor-bearing mice ( $n = 8$ ). Tumor-bearing mice were treated with vehicle or AR-42 (50 mg/kg, p.o., every other day) beginning at Day 6 post-tumor cell injection and ending at Day 17. Tumor-free control mice were treated with vehicle or AR-42 in parallel. Data are presented in box-and-whisker plots. The bottom and top of each box represent the first and third quartiles, and the “+” symbol and the band inside each box denote the mean and median values, respectively. The ends of the whiskers represent the maximum and minimum values in each group.

(IL-6R $\alpha$ ) were elevated in muscle of tumor-bearing/vehicle mice ( $n = 9$ ;  $P < .001$ ), and AR-42 reduced this cachexia-induced increase by 85% ( $P < .001$ ,  $n = 10$ ) (Figure 5Aiii). These findings suggest that AR-42 inhibits muscle wasting, in part, by blocking IL-6 signaling.

#### RNA-seq Analysis

Principal component analysis (PCA) of the RNA-seq data was performed to visualize biologically meaningful transcriptome

variation between the study groups (see [Supplementary Methods](#), available online, for additional information). The PCA plot shows that the two-dimensional projection of the variation in the tumor-bearing/AR-42 group (Tumor/AR42) was much more similar to those of the tumor-free, noncachectic groups (Tumor-free/vehicle, Tumor-free/AR42) than to that of the cachectic tumor-bearing/vehicle group (Tumor/vehicle) (Figure 5B, left). This clustering of expression profiles suggests that AR-42

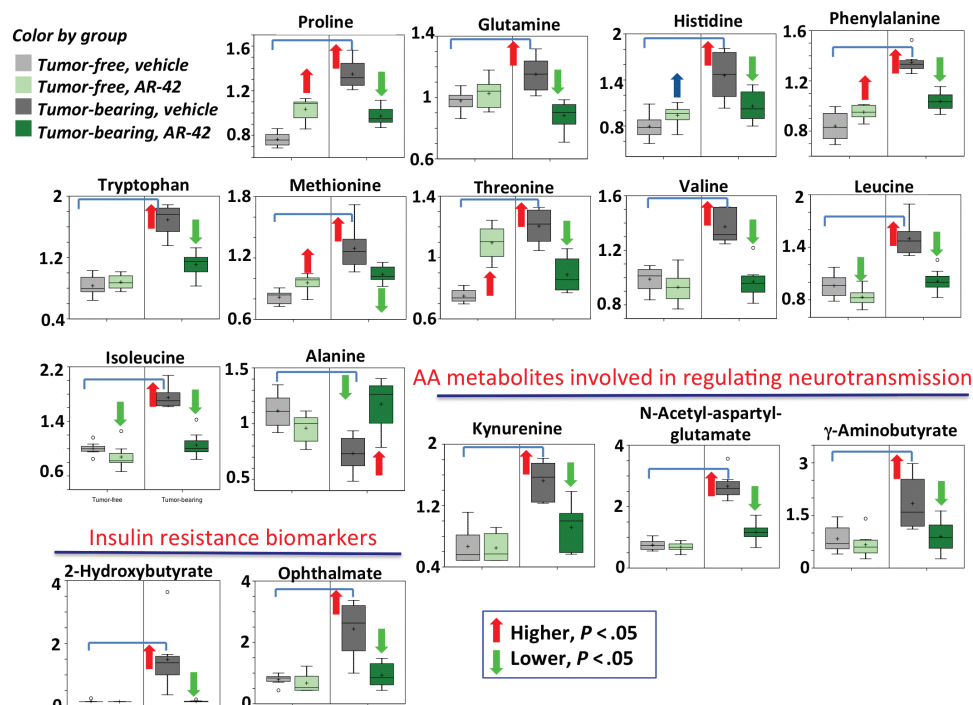


**Figure 4.** Effects of AR-42 on cachexia-induced changes in the levels of free amino acids, amino acid metabolites involved in regulating neurotransmission, and biomarkers of insulin resistance in skeletal muscle of C-26 tumor-bearing mice. Analyses were performed on gastrocnemius muscles from tumor-free and tumor-bearing mice ( $n = 8$ ). Tumor-bearing mice were treated with vehicle or AR-42 (50 mg/kg, p.o., every other day) beginning at Day 6 post-tumor cell injection and ending at Day 17. Tumor-free control mice were treated with vehicle or AR-42 in parallel. Data are presented in box-and-whisker plots. The bottom and top of each box represent the first and third quartiles, and the “+” symbol and the band inside each box denote the mean and median values, respectively. The ends of the whiskers represent the maximum and minimum values in each group.

reverted the transcriptome profile of muscle in the tumor-bearing/vehicle group to a state similar to that of noncachectic mice.

Pairwise comparisons of RNA-seq data were performed to identify genes differentially expressed between tumor-bearing/vehicle mice, representing the cachectic state, and each of the other three treatment groups, representing noncachectic states (tumor-free/vehicle and tumor-free/AR42), and the experimental state (tumor-bearing/AR-42). Of the total number of differentially expressed genes detected (9125), 4566 genes were shared among the three comparisons and 99.6% of those (4546 of 4566) shared the same direction of change (Figure 5B, right). This finding suggests that the tumor-bearing/AR-42 mice have a gene expression profile that is similar to those of the noncachectic groups and supports the notion that AR-42 shifted gene expression in cachectic muscle to a state similar to that in noncachectic muscle.

Pairwise comparison of gene expression in muscles from vehicle- and AR-42-treated tumor-bearing mice revealed a total of 677 genes with four-fold or greater differential expression (376 upregulated and 301 downregulated) (Supplementary Table 3, available online). Ingenuity Pathway Analysis (IPA) revealed that 66 of these genes were annotated to categories of atrophy, contractility, development, and muscle morphology, and skeletal muscle cell size, muscle cell death, and protein catabolism (Table 1).

Of these muscle function- and disease-associated genes, six are noteworthy in their links with cancer-induced cachexia. These include *Foxo1* (encoding Forkhead box protein O1) (7,23–25) and its target genes *Trim63* (MuRF1) and *Fbxo32* (Atrogin-1) (26,27), *PNPLA2* (adipose triglyceride lipase) (28,29), *UCP3* (uncoupling protein 3) (30,31), and *Mef2c* (myogenic transcription factor

myocyte enhancer factor) (32) (Figure 5C). In cachectic muscle from tumor-bearing/vehicle mice, the abundance of *Foxo1*, *Trim63*, *Fbxo32*, and *PNPLA2* transcript was elevated relative to that from tumor-free/control mice ( $P = .015$ ,  $P = .024$ ,  $P = .01$ , and  $P = .024$ , respectively), while that of *Mef2c* was decreased ( $P < .001$ ) (Figure 5C, Table 2). AR-42 restored expression of these genes to levels comparable to the noncachectic state (*Foxo1*,  $P = .007$ ; *Trim63*,  $P = .026$ ; *Fbxo32*,  $P = .012$ ; *PNPLA2*,  $P = .028$ ; and *Mef2c*,  $P = .014$ ). Validation of these RNA-seq data by qRT-PCR showed that the two datasets closely paralleled each other (Figure 5D). In cachectic muscle, the mRNA levels of *Foxo1*, *Trim63*, *Fbxo32*, *PNPLA2*, as well as *UCP3*, were statistically significantly upregulated, while that of *Mef2c* was decreased ( $P < .001$  for all markers, vs tumor-free/vehicle). AR-42 restored mRNA expression to basal levels ( $P < .001$  vs tumor-bearing/vehicle).

### Effect of Delayed Treatment With AR-42 on Cancer Cachexia

In the preceding experiments, AR-42 treatment started early in disease progression when overt signs of wasting were undetectable. To investigate whether later initiation of AR-42 treatment remains protective against cachexia, C-26 tumor-bearing mice were treated with AR-42 starting at 6, 10, and 12 days after tumor cell injection.

Consistent with previous data (Figure 1), tumor-bearing/vehicle mice lost 19% of body weight (tumor excluded) by Day 17. Treatment with AR-42 starting at Day 6, 10, or 12 limited weight loss to 6%, 11%, and 12%, respectively (Figure 6A, left), without appreciable effects on tumor growth (Figure 6A, right). Moreover,

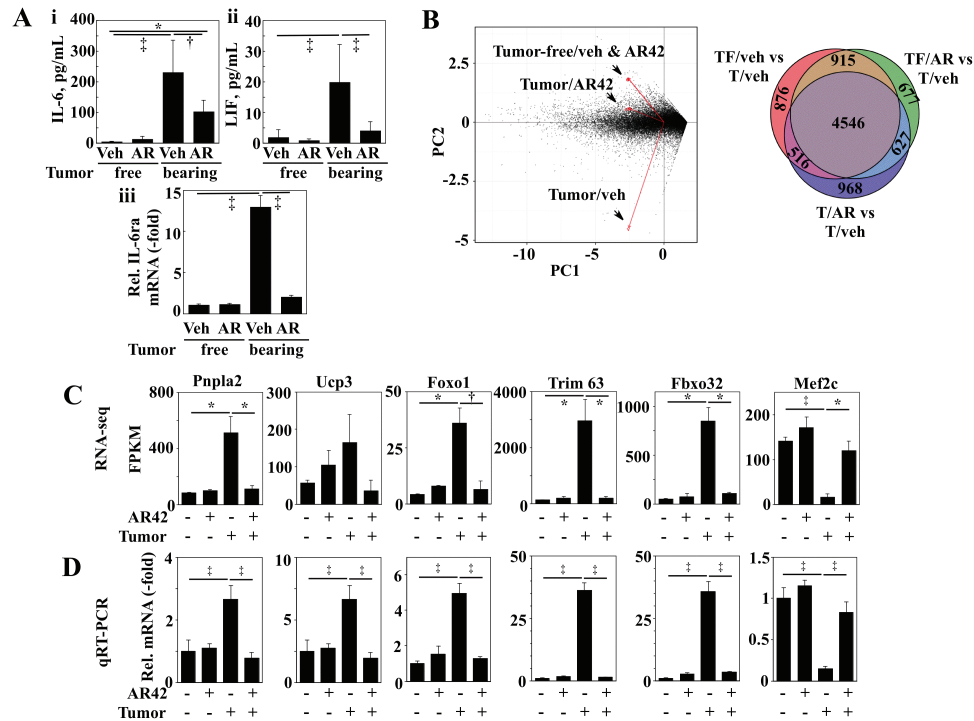


**Figure 5.** Cytokine profiling, RNA-seq, and quantitative real-time polymerase chain reaction (qRT-PCR) analyses of the effects of AR-42 on the expression of multiple procachexia drivers. Analyses were performed on sera or gastrocnemius muscles from tumor-free and tumor-bearing mice. Tumor-bearing mice were treated with vehicle or AR-42 (50 mg/kg, p.o., every other day) beginning at Day 6 post-tumor cell injection and ending at Day 17. Tumor-free control mice were treated with vehicle or AR-42 in parallel. **Ai and ii**) Effects of AR-42 on the levels of the procachexia cytokines IL-6 (i) and leukemia inhibitory factor (LIF) (ii) in the sera of vehicle- or AR-42-treated tumor-free vs C-26 tumor-bearing mice. **iii**) qRT-PCR analysis of the effects of AR-42 on the mRNA expression of IL-6Ra in skeletal muscle of vehicle- or AR-42-treated tumor-free vs C-26 tumor-bearing mice. Data are presented as means  $\pm$  SD (for [i] and [ii],  $n = 3$ ; for [iii],  $n = 8-10$ ). ( $^*P < .05$ ;  $^{\dagger}P < .01$ ;  $^{\#}P < .001$ ; analysis of variance [ANOVA]). **B** **Left**, two-dimensional projection of high-dimensional RNA-seq data from the four study groups. The principal component analysis axes (PC1, x-axis; PC2, y-axis) emphasize the overall variation in RNA-seq data. Labeled red vectors represent the overall transcriptome of each group. Each black dot represents a transformed gene expression value. **Right**, Venn diagram of differentially expressed genes in each of the three pairwise comparisons of cachectic (T/Veh) to noncachectic groups (TF/Veh, TF/AR, T/AR). The differentially expressed genes shared by all three comparisons (center portion, 4546 genes) changed expression in the same direction. T = tumor-bearing; AR = AR-42-treated; TF = tumor-free; veh = vehicle-treated. **C and D**) Analysis of the effects of AR-42 on the transcript levels of six key procachexia drivers by **(C)** RNA-seq ( $^*P < .05$ ;  $^{\dagger}P < .01$ ;  $^{\#}P < .001$ ;  $n = 3$ ) and **(D)** qRT-PCR ( $^{\#}P < .001$ ;  $n = 3$ ; ANOVA) in skeletal muscle of mice in the four treatment groups. Data are presented as means  $\pm$  SD. All statistical tests were two-sided.

AR-42-treated mice exhibited signs of better overall health and body condition than their vehicle-treated counterparts (Supplementary Figure 3, available online). AR-42 preserved gastrocnemius weight (mean  $\pm$  SD, tumor-bearing/vehicle,  $79.7 \pm 4.6\%$  of tumor-free/vehicle control; Day 6,  $94.4 \pm 4.1\%$ ; Day 10,  $90.9 \pm 6.3\%$ ; and Day 12,  $88.2 \pm 4.3\%$ ;  $P < .001$  for all treatment start times) and, to a lesser extent, those of tibialis anterior and quadriceps muscles (Figure 6B). Moreover, AR-42 preserved forelimb muscle strength in all drug-treated groups at Day 15 (mean  $\pm$  SD, tumor-bearing/vehicle,  $90.3 \pm 16.7$  N,  $P = .01$  vs tumor-free/vehicle [ $108.1 \pm 7.9$  N]; Day 6,  $109.1 \pm 14.6$  N,  $P = .022$ ; Day 10,  $117.7 \pm 10.3$  N,  $P < .001$ ; Day 12,  $110.9 \pm 4.5$  N,  $P = .002$ ) and Day 16 (tumor-bearing/vehicle,  $76.7 \pm 16.4$  N,  $P < .001$  vs tumor-free/vehicle [ $101.3 \pm 6.0$  N]; Day 6,  $99.6 \pm 11.6$  N; Day 10,  $102.9 \pm 11.6$  N; Day 12,  $104.8 \pm 8.4$  N;  $P < .001$  for all treatment start times) (Figure 6C).

## Discussion

Herein, we report the in vivo efficacy of AR-42 in suppressing muscle wasting in C-26 and LLC tumor models of cachexia. The pro-inflammatory cytokines, IL-6 and TNF, represent major procachectic factors in these models (33,34). While AR-42 had no effect on serum TNF levels in C-26 tumor-bearing mice, it reduced levels of serum IL-6 and intramuscular IL-6Ra mRNA expression. Nonetheless, IL-6 and IL-6Ra mRNA levels in AR-42-treated mice

remained higher than those in tumor-free mice, suggesting that decreased IL-6 signaling is not solely responsible for AR-42's anticachectic activity.

Mechanistically, the anticachectic effect of AR-42 appears unique, as the HDAC inhibitors valproic acid and trichostatin-A could not reverse muscle loss in C-26 tumor-bearing mice despite modulating the myostatin/follistatin axis (35). Similarly, we showed that, unlike AR-42, vorinostat and romidepsin could not attenuate cachexia-induced weight loss in the C-26 model. This discrepancy was associated with the greater ability of AR-42 to suppress the mRNA expression of Atrogin-1 and MuRF1 in the muscles of tumor-bearing mice, which may reflect differences in their respective abilities to modulate global gene expression in skeletal muscles.

Recent evidence suggests a mechanistic link between aberrant acetylation/expression of transcription factors and wasting in diseased muscles, through dysregulated expression of cachexia-associated genes (reviewed in [36]). Moreover, the histone acetyltransferase activity of p300/CBP differentially regulates transcriptional activity and nuclear localization of Foxo family transcription factors in skeletal muscles (37), and class I HDACs, especially HDAC1, play a crucial role in mediating nutrient deprivation- or muscle disuse-induced muscle atrophy by regulating expression of Foxo and its targets Atrogin-1 and MuRF1 (7). Interestingly, all three of the HDAC inhibitors

**Table 1.** Ingenuity Pathway Analysis of differentially expressed genes ( $\geq 4$ -fold)\* related to muscle disease or functions between AR-42- and vehicle-treated C-26 tumor-bearing mice (n = 3)

RefSeq ID	Gene ID	Log2 fold change	Description	Disease or function annotation
Upregulated by AR-42				
NM_024291	Ky	4.3	Kyphoscoliosis peptidase	Muscle development
NM_010267	Gdap1	4.2	Ganglioside-induced differentiation-associated-protein 1	Muscle atrophy; myopathy
NM_013569	Kcnh2	4.1	Potassium voltage-gated channel, subfamily H, member 2	Muscle atrophy; myopathy
NM_009608	Actc1	3.9	Actin, alpha, cardiac	Muscle development and morphology; myopathy; muscle cell death
NM_183408	Pde4a	3.7	Phosphodiesterase 4A, cAMP specific	Myopathy
NM_022322	Tnmd	3.5	Tenomodulin	Muscle morphology
NM_013803	Casr	3.5	Calcium-sensing receptor	Muscle cell death
NM_008596	Sypl2	3.5	Synaptophysin-like 2	Muscle contractility, development, and morphology; skeletal muscle cell size
NM_010518	Igfbp5	3.3	Insulin-like growth factor binding protein 5	Muscle development; skeletal muscle mass
NM_008876	Pld2	3.2	Phospholipase D2	Muscle cell death
NM_080440	Slc8a3	3.2	Solute carrier family 8 (sodium/calcium exchanger), member 3	Muscle cell death
NM_198190	Ntf5	3.2	Neurotrophin 5	Muscle development
NM_001170537	Mef2c	2.9	Myocyte enhancer factor 2C	Muscle contractility and development;
NM_176848	Fbxo2	2.8	F-box protein 2	Protein catabolism
NM_022027	Syne1	2.7	Synaptic nuclear envelope 1	Muscle development, function, and morphology; myopathy
NM_009255	Serpine2	2.6	Serine (or cysteine) peptidase inhibitor, clade E, member 2	Protein catabolism
NM_001256224	Wnt5a	2.6	Wingless-related MMTV integration site 5A	Protein catabolism
NM_134028	Tubg2	2.6	Tubulin, gamma 2	Myopathy
NM_021508	Myoz1	2.5	Myozenin 1	Muscle development and morphology; skeletal muscle mass and cell size
NR_110361	Cflar	2.5	CASP8 and FADD-like apoptosis regulator	Muscle morphology
NM_178608	Reep1	2.3	Receptor accessory protein 1	Myopathy
NM_001252455	Ptprs	2.3	Protein tyrosine phosphatase, receptor type, S	Muscle morphology; myopathy
NM_013491	Clcn1	2.3	Chloride channel 1	Muscle function
NM_008305	Hspg2	2.3	Perlecan (heparan sulfate proteoglycan 2)	Muscle development and morphology
NM_025358	Ndufa9	2.3	NADH dehydrogenase (ubiquinone) 1 alpha subcomplex, 9	Myopathy
NM_011436	Sorl1	2.3	Sortilin-related receptor, LDLR class A repeats-containing	Muscle function
NM_001243009	Col6a3	2.3	Collagen, type VI, alpha 3	Muscle development; myopathy
NM_025343	Rmnd1	2.3	Required for meiotic nuclear division 1 homolog (S. cerevisiae)	Myopathy
NM_001289762	Rarb	2.2	Retinoic acid receptor, beta	Muscle cell death
NM_021355	Fmod	2.1	Fibromodulin	Muscle morphology
NM_013645	Pvalb	2.1	Parvalbumin	Muscle contractility and development
NM_172259	Myl6b	2.1	Myosin, light polypeptide 6B	Muscle development
NM_008551	Mapkapk2	2.1	MAP kinase-activated protein kinase 2	Muscle cell death
NM_013712	Itgb1bp2	2.1	Integrin beta 1 binding protein 2	Muscle development
NM_021566	Jph2	2.1	Junctophilin 2	Muscle development and morphology; myopathy
NM_025823	Pcyox1	2.0	Prenylcysteine oxidase 1	Protein catabolism
NM_001013833	Prkg1	2.0	Protein kinase, cGMP-dependent, type I	Muscle contractility and function
NM_019735	Apip	2.0	APAF1 interacting protein	Muscle cell death
NM_009022	Aldh1a2	2.0	Aldehyde dehydrogenase family 1, subfamily A2	Muscle development and morphology
NM_008524	Lum	2.0	Lumican	Muscle morphology
Downregulated by AR-42				
NM_138677	Edem1	-2.0	ER degradation enhancer, mannosidase alpha-like 1	Protein catabolism
NM_001163704	Fbxo6	-2.0	F-box protein 6	Protein catabolism

Table 1. Continued

RefSeq ID	Gene ID	Log2 fold change	Description	Disease or function annotation
NM_011724	Xirp1	-2.1	Xin actin-binding repeat containing 1	Muscle contractility, development, and morphology
NM_001111099	Cdkn1a	-2.1	Cyclin-dependent kinase inhibitor 1A (P21)	Muscle development and morphology; skeletal muscle mass and cell size; muscle cell death
NM_001199733	Daxx	-2.1	Fas death domain-associated protein	Muscle cell death
NM_001081044	Mylk2	-2.1	Myosin, light polypeptide kinase 2, skeletal muscle	Muscle development; myopathy
NM_016736	Nub1	-2.1	Negative regulator of ubiquitin-like proteins 1	Protein catabolism
NM_007582	Cacng1	-2.2	Calcium channel, voltage-dependent, gamma subunit 1	Muscle development; protein catabolism
NM_020033	Ankrd2	-2.2	Ankyrin repeat domain 2 (stretch responsive muscle)	Muscle function and morphology
NM_172845	Adamts4	-2.2	A disintegrin-like and metallopeptidase (repolysin type) with thrombospondin type 1 motif, 4	Muscle development; protein catabolism
NM_009464	Ucp3	-2.2	Uncoupling protein 3	Skeletal muscle mass
NR_028142	Pnpla2	-2.2	Patatin-like phospholipase domain containing 2	Muscle morphology; muscle cell death
NR_104580	Slc8a1	-2.3	Solute carrier family 8 (sodium/calcium exchanger), member 1	Muscle development and morphology; muscle cell death; myopathy
NM_008871	Serpine1	-2.3	Serine (or cysteine) peptidase inhibitor, clade E, member 1	Muscle development
NM_001081185	Flnc	-2.3	Filamin C, gamma (actin binding protein 280)	Muscle development and morphology; myopathy
NM_009238	Sox4	-2.3	SRY-box containing gene 4	Muscle development and morphology
NM_001289716	Bcl2l1	-2.4	Bcl2-like 1	Muscle cell death and morphology; myopathy
NM_001165894	Akt1	-2.4	Thymoma viral proto-oncogene 1	Muscle atrophy, development, and function; skeletal muscle cell size; myopathy; protein catabolism
NM_007428	Agt	-2.5	Angiotensinogen (serpin peptidase inhibitor, clade A, member 8)	Muscle atrophy; smooth muscle mass; muscle cell death; myopathy; protein catabolism
NM_019739	Foxo1	-2.5	Forkhead box O1	Muscle atrophy and development; skeletal muscle mass; muscle cell death; myopathy
NM_013560	Hspb1	-2.5	Heat shock protein 1	Muscle atrophy; muscle cell death; myopathy
NM_026346	Fbxo32	-3.0	F-box protein 32	Muscle atrophy; myopathy; protein catabolism
NM_001159324	Gaa	-3.0	Glucosidase, alpha, acid	Muscle atrophy, development, function, and morphology; myopathy
NM_008244	Hgs	-3.3	HGF-regulated tyrosine kinase substrate	Protein catabolism
NM_013468	Ankrd1	-3.6	Ankyrin repeat domain 1 (cardiac muscle)	Muscle development, function, and morphology; muscle cell death
NM_001039048	Trim63	-3.9	Tripartite motif-containing 63	Muscle contractility and morphology; skeletal muscle mass and cell size; muscle atrophy; myopathy
NM_008491	Lcn2	-4.9	Lipocalin 2	Muscle cell death

\* Changes in expression of all genes listed are statistically significant at a q-value of <0.05.

examined in this study can inhibit HDAC1. Romidepsin is considered an inhibitor of class I HDACs (HDAC1, 2, 3, and 8), while vorinostat is a pan-HDAC inhibitor with activity against class I, class II (HDAC4, 5, 7, and 9 in subclass IIA, HDAC6 and 10 in subclass IIB), and class IV (HDAC11) HDACs (reviewed in [38]). AR-42 is also a paninhibitor, with activity against class I and IIB HDACs. Thus, HDAC specificity alone cannot account for the anticachectic effects of AR-42 compared with the other agents.

The situation is complicated by the fact that isoform specificities are conventionally determined using immunoprecipitated or recombinant proteins or catalytic subunits in cell-free conditions, whereas intracellular HDAC activity often occurs in the context of multiprotein complexes that can include other HDACs (39). Indeed, it was recently reported that the effects of various HDAC inhibitors differed depending on whether they were screened against purified HDAC enzymes or endogenous

**Table 2.** Ingenuity Pathway Analysis of differentially expressed genes ( $\geq 4$ -fold) related to muscle disease or functions between vehicle-treated C-26 tumor-bearing and tumor-free mice (n = 3)

RefSeq ID	Gene ID	Log2 fold change	Description	Disease or function annotation
Upregulated in tumor-bearing mice				
NM_011104	Prkce	10.1	Protein kinase C, epsilon	Damage of muscle cell lines
NM_008491	Lcn2	6.7	Lipocalin 2	Muscle cell death
NM_001111099	Cdkn1a	5.0	Cyclin-dependent kinase inhibitor 1A (P21)	Muscle development and morphology; skeletal muscle mass and cell size; muscle cell death
NM_001039048	Trim63	4.6	Tripartite motif-containing 63	Muscle contractility and morphology; skeletal muscle mass and cell size; muscle atrophy; myopathy
NM_013468	Ankrd1	4.5	Ankyrin repeat domain 1 (cardiac muscle)	Muscle development, function, and morphology; muscle cell death
NM_007428	Agt	3.7	Angiotensinogen (serpin peptidase inhibitor, clade A, member 8)	Muscle atrophy; smooth muscle mass; muscle cell death; myopathy; protein catabolism
NM_011724	Xirp1	3.4	Xin actin-binding repeat containing 1	Muscle contractility, development, and morphology
NM_019739	Foxo1	3.1	Forkhead box O1	Muscle atrophy and development; skeletal muscle mass; muscle cell death; myopathy
NM_008064	Gaa	3.1	Glucosidase, alpha, acid	Muscle atrophy, development, function, and morphology; myopathy
NM_013560	Hspb1	3.1	Heat shock protein 1	Muscle atrophy; muscle cell death; myopathy
NM_009238	Sox4	2.8	Sry-box containing gene 4	Muscle development and morphology
NM_001165894	Akt1	2.7	Thymoma viral proto-oncogene 1	Muscle atrophy, development, and function; skeletal muscle cell size; myopathy; protein catabolism
NM_009743	Bcl2l1	2.7	Bcl2-like 1	Muscle cell death and morphology; myopathy
NM_001081185	Flnc	2.7	Filamin C, gamma (actin binding protein 280)	Muscle development and morphology; myopathy
NM_011406	Slc8a1	2.6	Solute carrier family 8 (sodium/calcium exchanger), member 1	Muscle development and morphology; muscle cell death; myopathy
NM_001163689	Pnpla2	2.6	Patatin-like phospholipase domain containing 2	Muscle morphology; muscle cell death
NM_020033	Ankrd2	2.5	Ankyrin repeat domain 2 (stretch responsive muscle)	Muscle function and morphology
NM_008654	Ppp1r15a	2.5	Protein phosphatase 1, regulatory (inhibitor) subunit 15A	Muscle cell death
NM_008871	Serpine1	2.4	Serine (or cysteine) peptidase inhibitor, clade E, member 1	Muscle development
NM_011377	Sim2	2.3	Single-minded homolog 2 (Drosophila)	Skeletal muscle hypoplasia
NM_001199733	Daxx	2.3	Fas death domain-associated protein	Muscle cell death
Downregulated in tumor-bearing mice				
NM_011436	Sorl1	-2.0	Sortilin-related receptor, Ldlr class A repeats-containing	Muscle function
NM_172259	Myl6b	-2.1	Myosin, light polypeptide 6B	Muscle development
NM_008524	Lum	-2.3	Lumican	Muscle morphology
NM_011784	Aplnr	-2.4	Apelin receptor	Muscle function
NM_001252453	Ptprs	-2.5	Protein tyrosine phosphatase, receptor type, S	Muscle morphology; myopathy
NM_001013833	Prkg1	-2.6	Protein kinase, cGMP-dependent, type I	Muscle contractility and function
NM_001198790	Ak1	-2.8	Adenylate kinase 1	Muscle function
NM_021355	Fmod	-2.9	Fibromodulin	Muscle morphology
NM_001205076	Jph2	-2.9	Junctophilin 2	Muscle development and morphology; myopathy
NM_001170537	Mef2c	-3.1	Myocyte enhancer factor 2C	Muscle contractility and development
NM_021508	Myoz1	-3.2	Myozenin 1	Muscle development and morphology; skeletal muscle mass and cell size
NM_153399	Syne1	-3.3	Synaptic nuclear envelope 1	Muscle development, function, and morphology; myopathy

Table 2. Continued

RefSeq ID	Gene ID	Log2 fold change	Description	Disease or function annotation
NM_001167920	Slc8a3	-3.4	Solute carrier family 8 (sodium/calcium exchanger), member 3	Muscle cell death
NM_010518	Igfbp5	-3.7	Insulin-like growth factor binding protein 5	Muscle development; skeletal muscle mass
NM_008596	Sypl2	-4.2	Synaptophysin-like 2	Muscle contractility, development, and morphology; skeletal muscle cell size
NM_001039510	Adora1	-4.3	Adenosine A1 receptor	Damage of muscle cell lines
NM_009813	Casq1	-4.6	Calsequestrin 1	Muscle development
NM_009608	Actc1	-4.6	Actin, alpha, cardiac	Muscle development and morphology; myopathy; muscle cell death
NM_022322	Tnmd	-5.5	Tenomodulin	Muscle morphology
NM_024291	Ky	-5.6	Kyphoscoliosis peptidase	Muscle development

\* Changes in expression of all genes listed are statistically significant at a q-value of <0.05.

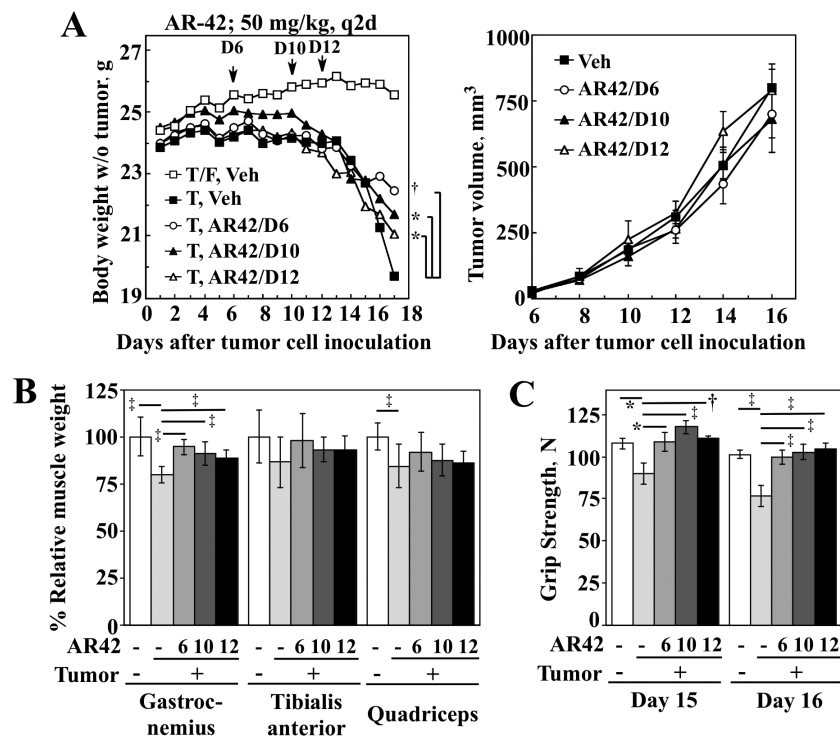


**Figure 6.** Effects of delaying treatment with AR-42 until late stages of tumor and cachexia progression in C-26 tumor-bearing mice. **A)** Left, changes in body weight (tumor excluded) in vehicle-treated tumor-free control mice (T/F, Veh) and tumor-bearing mice treated with vehicle (T, Veh) vs those treated with oral AR-42 starting at Day 6 (T, AR42/D6), Day 10 (T, AR42/D10), or Day 12 (T, AR42/D12) after tumor cell injection. Arrows indicate the time points for the start of AR-42 treatment. Data are presented as means (\* $P < .05$ ; † $P < .01$ ;  $n = 8$ ; analyzed using mixed effects model incorporating repeated measures for each subject with treatment and days as fixed factors). For clarity of presentation, the SD bars for each data point are not shown. Right, lack of suppressive effect of AR-42 on tumor growth in C-26 tumor-bearing mice in the delayed treatment experiment. Data are presented as means  $\pm$  SD ( $n = 8$ ). **B)** Effects of AR-42 treatment, initiated at different stages of disease progression as described in **(A)**, on the weights of gastrocnemius, tibialis anterior, and quadriceps muscles in C-26 tumor-bearing mice. Data are presented as means  $\pm$  SD ( $n = 8$ ; † $P < .001$ ; analysis of variance [ANOVA]). **C)** Effects of AR-42 on grip strength of tumor-bearing mice relative to the vehicle-treated tumor-free and tumor-bearing controls at Day 15 and Day 16 post-tumor cell injection. Data are presented as means  $\pm$  SD ( $n = 8$ ; \* $P < .05$ ; † $P < .01$ ; ‡ $P < .001$ ; ANOVA). All statistical tests were two-sided. N = Newtons.

HDAC-containing complexes (40). A more complete understanding of the mechanism underlying effects of HDAC inhibitors in muscle may need to account for such higher-order complexes.

RNA-seq analysis showed that AR-42 could reverse tumor-induced shifts in muscle gene expression. A total of 677 genes were differentially expressed by four-fold or greater between AR-42- and vehicle-treated tumor-bearing mice. Conceivably, this differential expression might arise from AR-42-mediated

effects on the transcriptional activity and/or expression of multiple transcription factors/regulators. In addition to Foxo1, AR-42 modulated the expression of many other transcription factors/regulators, including C/EBP $\delta$ , Fos, Jun-b, DAXX, ERN1, HIF3 $\alpha$ , MAFF, MAFK, and Mef2c. The importance of Mef2c in the development of skeletal, cardiac, and smooth muscle is well documented (41), and the AP-1 signaling cascade has been implicated in cancer-associated muscle wasting (42).

It has been proposed that cachectic muscles in C-26 tumor-bearing mice exhibit tumor Warburg physiology, characterized by a high rate of glycolysis (43). Our metabolomic data revealed a pronounced reprogramming of skeletal muscle metabolism in C-26 tumor-bearing mice, which was completely reversed by AR-42. The suppression of 2-hydroxybutyrate and ophthalmate, biomarkers for insulin resistance (20) and oxidative stress (21), by AR-42 is noteworthy, as substantial evidence has associated these conditions with cachexia (44–46). Similar to our findings in the skeletal muscles of tumor-bearing mice, the profiling of urinary metabolites in human cancer patients revealed that the presence of free amino acids, including branched-chain amino acids, such as valine, leucine, and isoleucine, was associated with skeletal muscle loss (47). Moreover, an elevated level of urine glucose was also detected, which was speculated to be suggestive of early insulin resistance, and is in line with the elevation of 2-hydroxybutyrate detected in our study. Thus, similarities between the metabolome of human cancer patients undergoing muscle loss (47) and that of C-26 tumor-bearing mice appear to exist, despite the difference in the biological material analyzed (urine vs skeletal muscle). Metabolomic analysis of urine may provide a noninvasive tool to monitor muscle loss during the clinical assessment of novel agents for cancer cachexia treatment.

Limitations of this study include the lack of clear understanding of how the preservation of metabolic homeostasis and gene expression is related mechanistically to the suppression of tumor-induced MuRF-1 and Atrogin-1 expression in the skeletal muscle of AR-42-treated C-26 tumor-bearing mice. Another limitation is that, although AR-42 had minimal effects on tumor burden, its effects on tumor-specific factors and their contribution to the inhibition of cachexia remain unknown. In addition, the dose of AR-42 and the treatment schedule used in this study were based on the effective tumor-suppressive regimen established previously in various xenograft models (8–11). Whether lower doses and/or a less intensive treatment schedule could elicit similar anticachectic effects was not evaluated here and, thus, could be considered another limitation. Evaluation of the anticachectic efficacy of AR-42 at lower doses is currently in progress. Such information is important as preclinical data are collected to support anticipated clinical trials in cancer patients in which AR-42 will be administered in combination with established chemotherapeutic regimens.

Mechanistically, the ability of AR-42 to maintain the integrity of skeletal muscles in tumor-bearing mice arises from its diverse, cumulative effects on tumor-induced changes in multiple transcriptional programs and metabolic phenotype. It is of therapeutic significance that oral administration of AR-42 at a late stage of tumor growth could slow the progression of muscle wasting in C-26 tumor-bearing mice. Together, these findings support further investigation of AR-42 as part of a comprehensive therapeutic strategy for cancer cachexia.

## Funding

This work was supported by the Lucius A. Wing Chair Endowed Chair Fund (to CSC) and a pancreatic cancer research grant from The Ohio State University Wexner Medical Center and Comprehensive Cancer Center (to TBS).

## Notes

The study funders had no role in the design of the study; the collection, analysis, or interpretation of the data; the writing of the manuscript; nor the decision to submit the manuscript for publication.

The authors thank Dr. Ralf Bundschuh (The Ohio State University) for guidance in the RNA-seq data analysis.

## References

1. Fearon KC, Glass DJ, Guttridge DC. Cancer cachexia: mediators, signaling, and metabolic pathways. *Cell Metab*. 2012;16(2):153–166.
2. Tisdale MJ. Cachexia in cancer patients. *Nat Rev Cancer*. 2002;2(11):862–871.
3. von Haehling S, Anker SD. Cachexia as a major underestimated and unmet medical need: facts and numbers. *J Cachexia Sarcopenia Muscle*. 2010;1(1):1–5.
4. Tisdale MJ. Mechanisms of cancer cachexia. *Physiol Rev*. 2009;89(2):381–410.
5. Lee SJ, Glass DJ. Treating cancer cachexia to treat cancer. *Skelet Muscle*. 2011;1(1):2.
6. Maccio A, Madeddu C, Mantovani G. Current pharmacotherapy options for cancer anorexia and cachexia. *Expert Opin Pharmacother*. 2012;13(17):2453–2472.
7. Beharry AW, Sandesara PB, Roberts BM, Ferreira LF, Senf SM, Judge AR. HDAC1 activates FoxO and is both sufficient and required for skeletal muscle atrophy. *J Cell Sci*. 2014;127(Pt 7):1441–1453.
8. Kulp SK, Chen CS, Wang DS, Chen CY, Chen CS. Antitumor effects of a novel phenylbutyrate-based histone deacetylase inhibitor, (S)-HDAC-42, in prostate cancer. *Clin Cancer Res*. 2006;12(17):5199–5206.
9. Lu YS, Kashida Y, Kulp SK, et al. Efficacy of a novel histone deacetylase inhibitor in murine models of hepatocellular carcinoma. *Hepatology*. 2007;46(4):1119–1130.
10. Sargeant AM, Rengel RC, Kulp SK, et al. OSU-HDAC42, a histone deacetylase inhibitor, blocks prostate tumor progression in the transgenic adenocarcinoma of the mouse prostate model. *Cancer Res*. 2008;68(10):3999–4009.
11. Yang YT, Balch C, Kulp SK, Mand MR, Nephew KP, Chen CS. A rationally designed histone deacetylase inhibitor with distinct antitumor activity against ovarian cancer. *Neoplasia* 2009;11(6):552–563, 3 p following 63.
12. Acharyya S, Ladner KJ, Nelsen LL, et al. Cancer cachexia is regulated by selective targeting of skeletal muscle gene products. *J Clin Invest*. 2004;114(3):370–378.
13. Verbeke G, Molenberghs G. *Linear Mixed Models for Longitudinal Data*. 1<sup>st</sup> ed. New York, NY: Springer-Verlag; 2000.
14. Holm S. A simple sequentially rejective multiple test procedure. *Scand J Statist*. 1979;6(2):65–70.
15. Mundy-Bosse BL, Lesinski GB, Jaime-Ramirez AC, et al. Myeloid-derived suppressor cell inhibition of the IFN response in tumor-bearing mice. *Cancer Res*. 2011;71(15):5101–5110.
16. Lucas DM, Alinari L, West DA, et al. The novel deacetylase inhibitor AR-42 demonstrates pre-clinical activity in B-cell malignancies in vitro and in vivo. *PLoS One*. 2010;5(6):e10941.
17. Sasaki Y, Naoe Y, Inoue T, et al. Effects of FK228, a novel histone deacetylase inhibitor, on human lymphoma U-937 cells in vitro and in vivo. *Biochem Pharmacol*. 2002;64(7):1079–1090.
18. Bodine SC, Latres E, Baumhueter S, et al. Identification of ubiquitin ligases required for skeletal muscle atrophy. *Science*. 2001;294(5547):1704–1708.
19. Lecker SH, Jagoe RT, Gilbert A, et al. Multiple types of skeletal muscle atrophy involve a common program of changes in gene expression. *FASEB J*. 2004;18(1):39–51.
20. Gall WE, Beebe K, Lawton KA, et al. alpha-hydroxybutyrate is an early biomarker of insulin resistance and glucose intolerance in a nondiabetic population. *PLoS One*. 2010;5(5):e10883.
21. Soga T, Baran R, Suematsu M, et al. Differential metabolomics reveals ophthalmic acid as an oxidative stress biomarker indicating hepatic glutathione consumption. *J Biol Chem*. 2006;281(24):16768–16776.
22. Tisdale MJ. Biology of cachexia. *J Natl Cancer Inst*. 1997;89(23):1763–1773.
23. Kamei Y, Miura S, Suzuki M, et al. Skeletal muscle FOXO1 (FKHR) transgenic mice have less skeletal muscle mass, down-regulated Type I (slow twitch/red muscle) fiber genes, and impaired glycemic control. *J Biol Chem*. 2004;279(39):41114–41123.
24. Reed SA, Sandesara PB, Senf SM, Judge AR. Inhibition of FoxO transcriptional activity prevents muscle fiber atrophy during cachexia and induces hypertrophy. *FASEB J*. 2012;26(3):987–1000.
25. Sandri M, Sandri C, Gilbert A, et al. Foxo transcription factors induce the atrophy-related ubiquitin ligase atrogin-1 and cause skeletal muscle atrophy. *Cell*. 2004;117(3):399–412.
26. Gumucio JP, Mendias CL. Atrogin-1, MuRF-1, and sarcopenia. *Endocrine*. 2013;43(1):12–21.
27. Bonaldo P, Sandri M. Cellular and molecular mechanisms of muscle atrophy. *Dis Model Mech*. 2013;6(1):25–39.
28. Das SK, Hoefler G. The role of triglyceride lipases in cancer associated cachexia. *Trends Mol Med*. 2013;19(5):292–301.
29. Young SG, Zechner R. Biochemistry and pathophysiology of intravascular and intracellular lipolysis. *Genes Dev*. 2013;27(5):459–484.
30. Collins P, Bing C, McCulloch P, Williams G. Muscle UCP-3 mRNA levels are elevated in weight loss associated with gastrointestinal adenocarcinoma in humans. *Br J Cancer*. 2002;86(3):372–375.
31. Constantinou C, Fontes de Oliveira CC, Mintzopoulos D, et al. Nuclear magnetic resonance in conjunction with functional genomics suggests mito-

- chondrial dysfunction in a murine model of cancer cachexia. *Int J Mol Med*. 2011;27(1):15–24.
32. Shum AM, Mahendradatta T, Taylor RJ, et al. Disruption of MEF2C signaling and loss of sarcomeric and mitochondrial integrity in cancer-induced skeletal muscle wasting. *Aging (Albany NY)*. 2012;4(2):133–143.
  33. Sherry BA, Gelin J, Fong Y, et al. Anticachectin/tumor necrosis factor- $\alpha$  antibodies attenuate development of cachexia in tumor models. *FASEB J*. 1989;3(8):1956–1962.
  34. Strassmann G, Fong M, Kenney JS, Jacob CO. Evidence for the involvement of interleukin 6 in experimental cancer cachexia. *J Clin Invest*. 1992;89(5):1681–1684.
  35. Bonetto A, Penna F, Minero VG, et al. Deacetylase inhibitors modulate the myostatin/follistatin axis without improving cachexia in tumor-bearing mice. *Curr Cancer Drug Targets*. 2009;9(5):608–616.
  36. Alamdari N, Aversa Z, Castillero E, Hasselgren PO. Acetylation and deacetylation--novel factors in muscle wasting. *Metabolism*. 2013;62(1):1–11.
  37. Senf SM, Sandesara PB, Reed SA, Judge AR. p300 Acetyltransferase activity differentially regulates the localization and activity of the FOXO homologues in skeletal muscle. *Am J Physiol Cell Physiol*. 2011;300(6):C1490–C1501.
  38. Lane AA, Chabner BA. Histone deacetylase inhibitors in cancer therapy. *J Clin Oncol*. 2009;27(32):5459–5468.
  39. Vaquero A, Scher M, Reinberg D. Biochemistry of multiprotein HDAC complexes. In: Verdin E, ed. *Histone Deacetylases: Transcriptional Regulation and Other Cellular Functions*. Totowa, NJ: Humana Press, Inc.; 2006:23–60.
  40. Bantscheff M, Hopf C, Savitski MM, et al. Chemoproteomics profiling of HDAC inhibitors reveals selective targeting of HDAC complexes. *Nat Biotechnol*. 2011;29(3):255–268.
  41. Black BL, Olson EN. Transcriptional control of muscle development by myocyte enhancer factor-2 (MEF2) proteins. *Annu Rev Cell Dev Biol*. 1998;14:167–196.
  42. Moore-Carrasco R, Garcia-Martinez C, Busquets S, et al. The AP-1/CJUN signaling cascade is involved in muscle differentiation: implications in muscle wasting during cancer cachexia. *FEBS Lett*. 2006;580(2):691–696.
  43. Der-Torossian H, Wysong A, Shadfar S, Willis MS, McDunn J, Couch ME. Metabolic derangements in the gastrocnemius and the effect of Compound A therapy in a murine model of cancer cachexia. *J Cachexia Sarcopenia Muscle*. 2013;4(2):145–155.
  44. Asp ML, Tian M, Wendel AA, Belury MA. Evidence for the contribution of insulin resistance to the development of cachexia in tumor-bearing mice. *Int J Cancer*. 2010;126(3):756–763.
  45. Honors MA, Kinzig KP. The role of insulin resistance in the development of muscle wasting during cancer cachexia. *J Cachexia Sarcopenia Muscle*. 2012;3(1):5–11.
  46. Moylan JS, Reid MB. Oxidative stress, chronic disease, and muscle wasting. *Muscle Nerve*. 2007;35(4):411–429.
  47. Eisner R, Stretch C, Eastman T, et al. Learning to predict cancer-associated skeletal muscle wasting from  $^1\text{H-NMR}$  profiles of urinary metabolites. *Metabolomics*. 2011;7(1):25–34.